Investigations of Pole Erosion Mechanisms in the 12.5 kW HERMeS Hall Thruster Using Numerical Simulations and Ion Velocity Measurements

Alejandro Lopez Ortega[1] and Ioannis G. Mikellides[2]
Jet Propulsion Laboratory, California Institute of Technology, Pasadena, CA, 91109, United States

Abstract: When the Hall Effect Rocket with Magnetic Shielding (HERMeS) was tested at the NASA GRC's VF-5 the erosion rate on the pole covers was found to be at least a factor of two higher at 300 V and 20.8 A than at other operating conditions in the 400 V to 600 V range. Simulations using our hydrodynamics code Hall2De do not predict increased erosion rates at 300 V but accurately compute erosion rates similar to the measurements at the other operating conditions. We investigate the source of the discrepancy between measurements and simulations at 300 V using a combination of numerical simulations and experimental measurements of the ion velocity fields in the acceleration region of the thruster. By examining previous simulations that predicted the measured erosion rates for other thrusters and operating conditions, we determine that sputtering of the pole surfaces by high energy ions is the most likely mechanism behind the erosion rates at 300 V. High energy ions sputter the pole surfaces when the acceleration region of the thruster is downstream of the pole surface plane. When the latter occurs, the curvature of the plasma potential contours at the edges of the channel accelerates a small fraction of the high energy ions radially. We find that neither our Hall2De simulations nor the experimental measurements produce ions of sufficiently high energy and flux to the inner pole cover to explain the measured erosion there. Only at the outer edge of the cover is where we find the ions needed to yield simulation results that are comparable to the erosion measurements. We argue that one possible mechanism for the higher erosion is high energy ions that graze the channel corner of the pole and become trapped in a sheath that develops downstream. Within the sheath, we find that the electric field is large enough to turn the ions towards the surface of the pole. A simplified calculation shows that the erosion rates produced by sputtering of trapped ions are similar to the measurements. We also propose that the presence of local oscillations and high-energy cathode ions may be sources of the enhanced erosion We conclude this article by proposing a combination of analysis, simulation, and experimental measurements that can be used to address the validity of these hypotheses.

I. Nomenclature

B = magnetic field
β = angular amplification factor of sputtering yield
e = elementary charge
ε_0 = vacuum permittivity
ε_s = energy of species s
$\dot{\varepsilon}_r$ = erosion rate
E = electric field
J_s = current of species s
j_s = current density of species s

[1] Member of the Technical Staff, Electric Propulsion Group, 4800 Oak Grove Drive, Pasadena, CA, 91109, Mail Stop 125-109, Member AIAA
[2] Principal Engineer, Electric Propulsion Group, 4800 Oak Grove Drive, Pasadena, CA, 91109, Mail Stop 125-109, Associate Fellow AIAA.

λ_{De} = Debye length
m_s = mass of species s
n_0 = plasma density
ϕ = plasma potential
r = radial coordinate
r_i = radial location of inner edge of pole cover
r_0 = radial location of outer edge of pole cover
T_s = temperature of species s
u_s = velocity of species s
ν = collision frequency
Y = sputtering yield
z = axial coordinate
a = (subscript) anomalous
e = (subscript) electrons
i = (subscript) ions
iz = (subscript) charge number of ions
iF = (subscript) fluid number for ions in multi-fluid simulation
n = (subscript) neutrals
// = (subscript) parallel
$\perp$ = (subscript) perpendicular

II. Introduction

The 12.5-kW Hall Effect Rocket with Magnetic Shielding (HERMeS) [1] is part of the Ion Propulsion System (IPS) under development through the Advanced Electric Propulsion System (AEPS) contract with Aerojet Rocketdyne. Work conducted at NASA Glenn Research Center (GRC) and Jet Propulsion Laboratory (JPL) aims to provide insight/oversight and testing support of the contract as well as risk reduction and life qualification activities [2-3]. The specification for HERMeS calls for 23 kh of operation of the propulsion system that must be demonstrated with a 50% margin. The thruster is operated at a nominal discharge current of 20.8 A and discharge voltage range of 300 to 600 V. Due in part to the unprecedented throughput requirements for the thruster, the life qualification plan calls for operation of the thruster in a vacuum facility for 23 kh and demonstration of the 50 % margin (11.5 kh) by physics-based modeling and simulation. Modeling and simulation has already been used in the program to provide valuable insight to observations from shorter wear tests [4] and will be used to support the 23-kh test.

The propellant throughput of Hall thrusters has been historically limited by the erosion of the acceleration channel walls, which inevitably leads to exposure of critical magnetic circuit components to the plasma. The magnetic field topology used in HERMeS was designed following the principles of magnetic shielding [5]. This technique acknowledges that the main cause of erosion in the discharge channel is the existence of plasma potential gradients and high electron temperatures that drive energetic ions towards the walls, and applies a design strategy for the magnetic field topology that avoids such conditions. In a succinct manner, a change in the topology of the magnetic field lines is sought such that they "graze" the channel walls instead of meeting them at an angle. It was shown in [6] that the lines of force in the Hall thruster channel are also isothermal lines, resulting in a potential distribution along them that closely follows the Boltzmann relation for electrons. By enforcing an electron temperature as cold as possible along the grazing lines, the plasma potential along the channel walls remains approximately constant, which in turn, precludes the acceleration of ions towards the walls. A proof-of-concept investigation of the magnetic shielding principles was conducted at the Jet Propulsion Laboratory in 2010-2012 [5,7-8] and involved the modification of 6 kW-class laboratory Hall thruster called H6 [9] from its original configuration, hereinafter termed H6US, to a magnetically shielded one (H6MS) with the guidance of modeling and simulation. A 150-hour wear test of the latter at nominal conditions (300 V, 20 A) revealed that erosion rates at the channel walls were 2 to 3 orders of magnitude lower than those found in the H6US. Wear tests [4] and numerical simulations [10] have also showed negligible erosion of the channel walls of HERMeS during operation.

The 150-hour wear test of the H6MS also revealed roughening of the inner and outer pole surfaces [11], a phenomenon that had not been observed in the unshielded version of the H6. This observation motivated a second wear test to measure the erosion along the poles. It was found that these erosion rates were at least an order of magnitude lower than at the channel walls in the H6US. Thus, erosion of the poles could simply be delayed for tens of thousands of hours by adding graphite covers of a few millimeters of thickness. This design feature was

subsequently incorporated in HERMeS thereby ensuring the thruster meets the throughput requirements. Since the pole cover erosion results for the H6MS became available, we have devoted significant modeling and simulation efforts to understand the mechanisms of pole erosion [10, 12]. More recently, a similar investigation was carried out for HERMeS with the aim to understand the differences in pole erosion observed in wear tests at different operating conditions [10]. The main conclusions of these investigations are summarized below.

The surface of the pole covers is exposed to multiple ion populations. One such population consists of ions that are generated in the plume of the centered mounted cathode. The density of this ion population decreases substantially away from the thruster centerline. These ions can carry significant kinetic energy if large wave instabilities exist in the cathode plume [13-14]. However, the operating parameters of the HERMeS cathode were chosen to minimize the presence of wave instabilities. As erosion rates depend linearly on ion current density, cathode plume ions are expected to affect more the inner edge of the inner front pole cover (i.e., the edge of the pole cover closer to the cathode) and the cathode keeper. It is more difficult to explain the existence of sputtering due to cathode ions at the outer edge of the inner pole and at the outer pole. Wear tests and simulations [10, 15] have showed that sputtering near the inner edge of the inner pole cover decreases when the cathode has a recessed position with respect to the cover surface in comparison to when the cathode exit is collinear with the cover surface. This phenomenon can be explained by the inner edge blocking the front surface from ions in the recessed configuration. Another population consists of ions that are generated by charge exchange or ionization in the vicinity of the pole cover. The rate of generation of ions in the vicinity of the poles is very low and these ions do not have enough energy to erode the pole surface significantly, as shown by LIF measurements conducted by Jorns et al. [16] for the H6MS. Most of the energy of these ions is acquired in the sheath, which exhibits a typical potential gradient of approximately 30 V, the latter value being comparable to the sputtering threshold of graphite (see Section III in [10]). Finally, energetic ions from the beam can also sputter the pole surface. These can be ions generated either in the ionization region of the discharge chamber, with energies comparable to the discharge voltage, or in the acceleration region and travel at lower velocities. However, the current density of these ions at the pole is typically small compared to the current density of less energetic ions. Efficient Hall thrusters are designed in a way such that most of the ion acceleration occurs in the axial direction and, thus, any radial acceleration can be considered a second-order effect. While ions generated in the ionization region can exhibit more diverse trajectories, these ions are not many in number as the acceleration region is very narrow axially (typically less than 20% of the channel length). In our investigations, we have identified that a more downstream location of the acceleration region is conductive to an increase in the sputtering of the poles by energetic ions as long as the plasma potential contours offer direct line-of-sight between the locations ion are generated and the pole surface. In Fig. 1, we show the streamtraces of high-energy ions (~250 V) from the H6MS and H6US simulations. In the H6MS, the acceleration region was more downstream than that in the H6US due to the more downstream location of the peak magnetic field (a consequence of the implementation of magnetic shielding). As the acceleration region in the H6MS moves outside of the acceleration channel, the plasma potential contours acquire a rounded shape at the edges of the channel. The latter allows for the acceleration in the radial direction of a sufficient amount of high energy ions to explain the erosion in the H6MS. This mechanism alone also explains the absence of pole sputtering in the H6US. The plasma can also move downstream as the result of global oscillations. In [10], we showed that HERMeS at 600 V exhibits large discharge current oscillations that translated into axial oscillations of the location of the acceleration region, which were in turn observed using laser-induced fluorescence (LIF) [17]. When these oscillations were accounted for in our simulations at 600 V, our computed erosion rates agreed well with the wear test results.

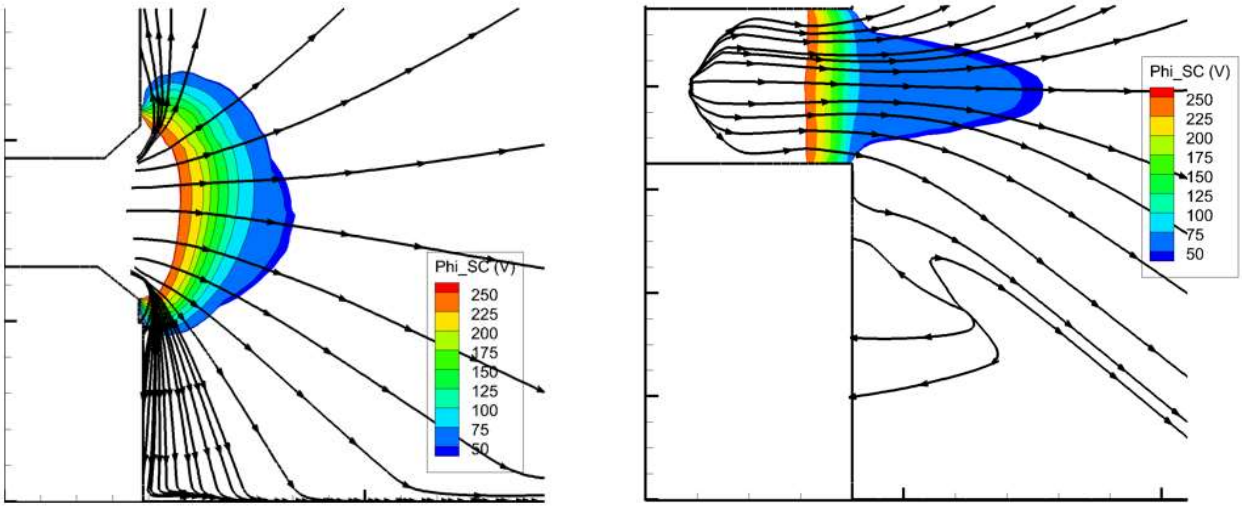

Figure 1. Streamtraces of 250-eV ions and plasma potential contours in the H6MS (left) and H6US (right)

In [10], we compared our numerical results on the erosion rates at the poles with those from the wear test for the throttling envelope of HERMeS (discharge voltage from 300 to 600 V and magnetic field strength from 75% to 125% of nominal). We found that the largest disagreement between simulations and experiments occurred at 300 V and at the nominal magnetic field condition (no experimental data was available at 300 V and non-nominal magnetic fields). The results of the wear tests at 300 V (Fig. 2) showed higher erosion, by approximately a factor of two with respect to the 600-V operating condition at the same discharge current. The measured erosion at the inner pole is also a factor of two higher than for the H6MS (except at the outer edge of the inner pole where they are comparable). Our simulations showed instead that the erosion rates did not increase at lower discharge voltages. Even though the LIF measurements of the ion distribution function in the acceleration region indicate that the location of maximum acceleration moves downstream with lower discharge voltage, we found that the acceleration region at 300 V was not downstream enough in our simulations to allow for the curvature of the potential at the edges of the channel to accelerate ions radially. In fact, we found that the acceleration region in HERMeS at 300 V is upstream of the acceleration region in the H6MS (Fig. 3). For simulations run at 75% of the nominal magnetic field strength at 300 V, we started observing some energetic ions sputtering the outer edge of the inner pole cover as the acceleration region moves downstream with respect to its location at nominal magnetic field. Considering all the evidence available and the fact that global oscillations are small at 300 V [10], the source of the disagreement between measurements and simulations could be traced back to three sources: uncertainty in the erosion measurements, uncertainty in the LIF measurements (used in [10] to inform the location of the acceleration region in our simulations), and sensitivity of the erosion on the plasma potential contours at the edges of the acceleration channel. The latter is motivated by the disagreement, discussed in [10] and observed between our simulations and the LIF measurements for a small number of locations away from the channel centerline. In order to address these concerns, an additional short-duration wear test campaign was launched to verify the erosion rates at 300 V and nominal magnetic field (Fig. 2, right) [18]. The wear test revealed in general slightly lower (by less than a factor of 1.5) erosion rates to those previously measured at nominal operating conditions. Erosion rates at the inner pole were also measured for a wear test conducted in a test facility at higher background pressure (10 μTorr vs 5 μTorr). The measured erosion profile is a factor of 1.5 to 2 lower than those found in tests at low background pressure. Attending at the typical error bars of the measurements in Fig. 2, it is difficult to determine whether the differences in these measurements are within the experimental uncertainty or suggest physical phenomena such as decreasing erosion rates at increased background pressure or high sensitivity of the results on the precise conditions the thruster is operated. The wear tests also concluded that erosion rates increased with magnetic field strength at 300 V (Fig. 2, left). This latter result contradicts the trends we observed in our simulations as the acceleration region moves upstream with increased magnetic strength, a phenomenon that should in principle not lead to increased sputtering by energetic ions. Additional LIF measurements were also conducted at GRC [19]. The comparison between the new LIF measurements and the previous measurements did not reveal significant differences in the location of the acceleration region either. These measurements were obtained with

a background pressure of approximately 10 μTorr. Chaplin et al. [17] found that changes in the location of the acceleration region when the background pressure was double were in the order of z/L=0.025. In order to address the uncertainty in the plasma potential contours at the edges of the beam, LIF measurements were also obtained off-centerline, providing a two-dimensional map of the velocity in the acceleration region that can be easily translated to plasma potential values (i.e., the previous campaign [17] did not obtain data at sufficient locations off-centerline to provide a two-dimensional map).

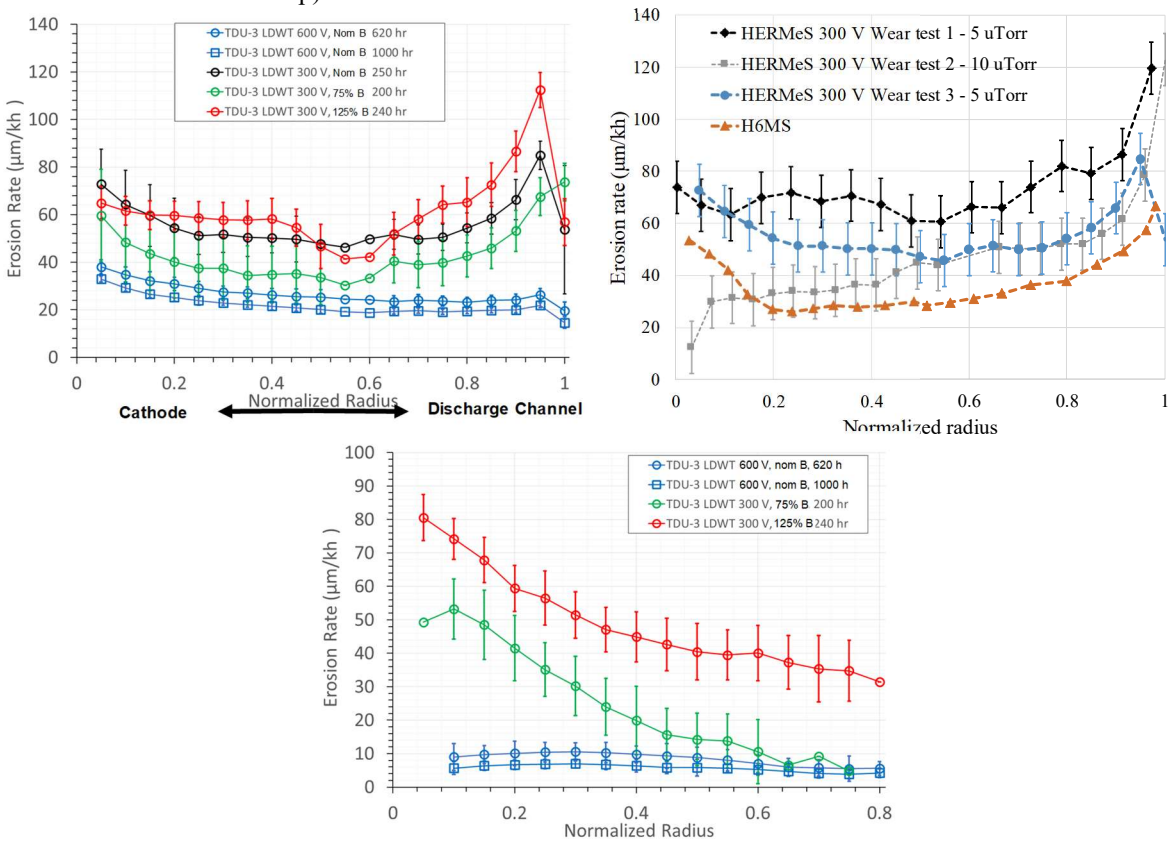

Figure 2. Left: Erosion rates along inner pole surface for 300 V operating conditions [18] and comparison with 600 V measurements. Right: Erosion rates for multiple measurements at 300 V – 20.8 A with nominal magnetic field and comparison with erosion rates for H6MS at 300 V – 20 A. Bottom: Erosion rates along outer pole surface for 300 V at 75% and 125% of nominal magnetic field and 600 V – 20.8 A with nominal magnetic field.

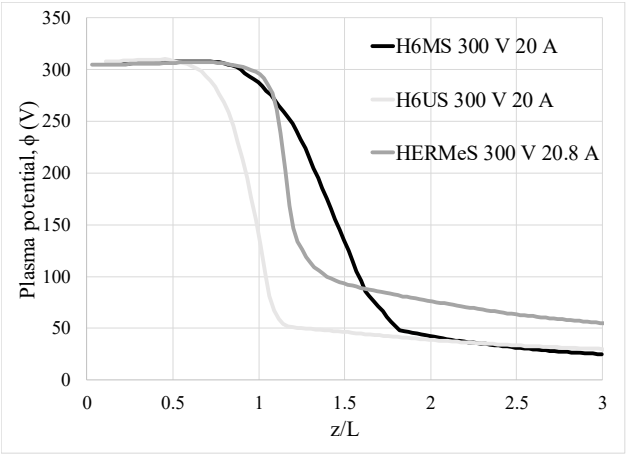

Figure 3. Comparison in location of acceleration region (defined loosely by the largest gradients in the plasma potential) for H6MS, H6US and HERMeS

In this article, we present an investigation whose aim is to gain understanding on the mechanisms that produce an increase in erosion rates at the 300 V operating condition. In Section III, we present a brief description of the equations included in Hall2De. In Section IV, we compare the two-dimensional contours of ion velocity and plasma potential in Hall2De to those extracted from LIF measurements and comment on the main differences we encounter and their effect on the predicted erosion rates. We determine that the measured ion velocity and plasma potential distribution cannot explain for themselves the erosion rates observed at the inner pole of HERMeS at 300 V – 20.8 A and nominal magnetic field. In Section V, we explore some mechanisms that may explain the measured erosion rates. Section VI summarizes the major findings of this article.

III. General description of Hall2De

Hall2De is a 2-D axisymmetric code for the simulation of the plasma discharge in Hall effect thrusters whose development began at the Jet Propulsion Laboratory about a decade ago. Its most notable features are described here whilst the interested reader can find the specifics of the numerical implementation in [20-21]. In Hall2De, a quadrilateral-based computational grid aligned with the magnetic field is employed. A typical simulation domain comprises the acceleration channel and a region of the plume that extends several times the length of the channel in the radial and axial directions. The dimensions of the computational domain enable a realistic simulation of the cathode plume (but not the hollow cathode interior). Cylindrical geometry is assumed, with the axis being the thruster centerline, in a way such that equations of motion are only solved in the axial and radial directions. This simplification is particularly beneficial in the case of centrally mounted cathodes. The motion of each of the species in the plasma is solved separately. The density and velocity field of neutral particles is modeled assuming free-molecular flow, using a view-factor algorithm described in [22]. Ions are modeled using multi-fluid hydrodynamics that can be combined with a particle-in-cell (PIC) method. This hybrid approach has been implemented to allow for resolving the multiple ion populations that sputter the pole cover. It was shown in [20] that ions generated in the channel have sufficiently long residence time compared to their collision time to warrant a Maxwellian distribution, which allows for hydrodynamic conservation equations. As this first population moves to the acceleration region, the residence time decreases and new ions cannot equilibrate with the bulk population. These new ions have a wide range of energies due to the steepness of the acceleration region and are difficult to model using a fluid approach. This is especially true for erosion calculations, since excessive energy averaging over the ion populations could lead to large errors due to the strong dependence of the sputtering yield on the ion energy. Thus, ions generated in the acceleration region and downstream are typically modeled with PIC though a multi-fluid approach can also produce similar accuracy if applied properly (i.e., when we can estimate the average energy of the ions sputtering the pole surface, we can choose thresholds for the energy between fluid ion populations accordingly). Finally, since ions produced by the cathode or generated in the cathode plume are dense and slow they can be modeled as an independent fluid. A typical Hall2De simulation will then consist of two populations modeled as separate fluids (i_F), one associated with the ionization region in the channel and the other with the cathode, and one population modeled with PIC for ions generated in the acceleration region and plume (Fig. 1). Separate continuity and momentum equations are solved for each fluid population and each charge state, i_Z. Ions of different i_F and i_Z numbers can interact with one another through ionization, charge exchange, and elastic collisions. The inclusion of multiple ion populations allows for more accurate erosion predictions and better tracking of the provenance of sputtering ions.

Electron motion makes use of a fluid approach where inertia is neglected. This approach results in a vector form of Ohm's law that is solved in the directions parallel

$$0 = -n_0 e E_{//} - \nabla_{//}(n_0 e T_e) - n_0 m_e \left((\nu_{ei}+\nu_{en})u_{e//} - \nu_{ei} u_{i//}\right), \tag{1}$$

and perpendicular to the magnetic field lines

$$0 = -n_0 e E_{\perp} - \frac{n_0 e^2 B^2 u_{e\perp}}{m_e(\nu_{ei}+\nu_{en}+\nu_a)} - \nabla_{\perp}(n_0 e T_e) - n_0 m_e\left((\nu_{ei}+\nu_{en}+\nu_a)u_{e\perp} - \nu_{ei} u_{i\perp}\right). \tag{2}$$

The anomalous collision frequency ν_a accounts for the anomalous transport of electrons known to persist in Hall thrusters. Eqs. (1-2) enable the computation of the plasma potential when combined with current conservation and the assumption of plasma quasi-neutrality. Finally, the electron temperature is determined as the solution of an energy

conservation equation [20]. We also include a (optional) space-charge algorithm that corrects the value of the plasma potential in regions where the Debye length becomes comparable to or larger than the size of the local computational grid [12]. Erosion rates at the walls of the thruster are computed from the ion current density and energy at the walls. The sputtering models used in our HERMeS investigations were described in detail in [10].

IV. Comparison between LIF measurements and numerical simulations for HERMeS at 300 V

A. Interpolation/extrapolation of LIF measurements to the Hall2De computational domain

Laser-induced fluorescence (LIF) [23-24] is an experimental technique that relies on excitation of xenon ions by the use of laser to determine the ion velocity distribution function in the direction parallel to the beam at discrete locations in the plasma. When two laser beams are employed, one can determine a two-dimensional distribution function (for instance, axial-radial in a Hall thruster) that can in turn be processed to evaluate the average velocity of ions. When this technique is applied to multiple locations in the plasma, one can extract a map of the ion velocity. If we assume that the ion velocity is mostly determined by the electrostatic force in a Hall thruster, plasma potential maps can be obtained making use of the expression:

$$\phi_{LIF}(z,r) = \phi_{ref} - \frac{m_i}{2e}\left(u_{iz,LIF}^2 + u_{ir,LIF}^2\right), \quad (3)$$

where ϕ_{ref} is the plasma potential at the stagnation point of the velocity in the ionization region (typically 5 to 10 V higher than the discharge voltage), and $u_{iz,LIF}$ and $u_{ir,LIF}$ are the velocity extracted from LIF measurements in the axial and radial directions, respectively.

Huang, et al. [19] conducted LIF measurements at GRC in a domain defined by a two-dimensional grid with axial and radial spacing between evaluation points of approximately 0.125L, with L being the length of the acceleration channel. Fig. 4 shows the locations at which these measurements were made, with red circles denoting locations for which reliable measurements do not exist. The latter can be due to low noise-to-signal ratios which occur in LIF measurements when the density of ions is low enough that the ion signal cannot be distinguished from the noise in the measurement, or due to relatively weak signals associated with low-density ion populations such as, for example, a high-energy population in a background of low energy ions. This latter phenomenon was already observed in the vicinity of the inner pole in the H6MS [16], a location for which a low energy and high energy population of ions exist. However, if the density of low energy ions is large, the signal produced by the high energy population can be masked. In addition to the locations showed in Fig. 4, measurements were made along the inner and outer pole surfaces at distances of 0.025L, 0.075L, 0.125L and 0.25L.

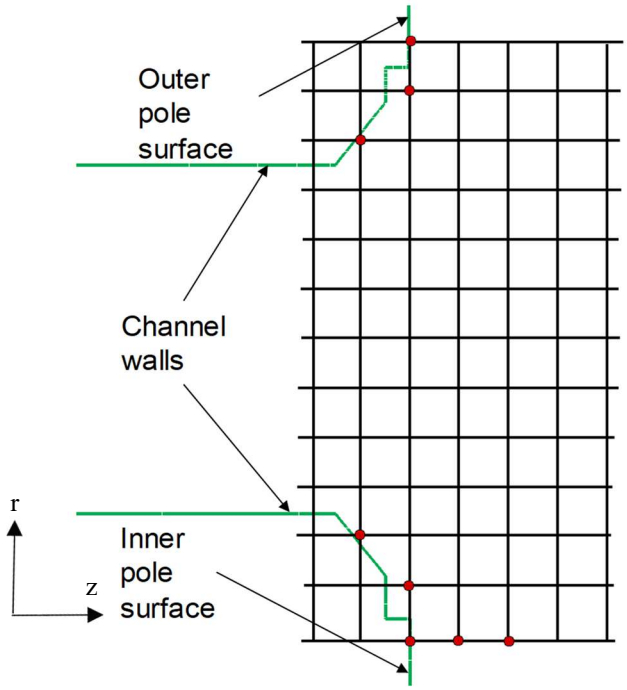

Figure 4. Location of LIF measurements with respect to Hall thruster geometry. Red circles indicate locations for which accurate measurements are not available for the HERMeS 300 V – 20.8 A – nominal magnetic field condition. Measurements are available at all other points except for those outside of the thruster

We notice from Fig. 4 that some of the points for which measurements are not reliable can be important to the determination of the shape of the plasma potential contours at the edges of the beam, which in turn have a direct effect on how ions are directed radially towards the pole regions. We followed two strategies to provide values of the plasma potential at these points. The first strategy consists of acknowledging that magnetic shielding will lead to plasma potentials at the walls of the channel that are close to 300 V. Thus, for each axial slice that has an unreliable point, we assume that the plasma potential is 300 V at the location close to the wall and then assume linear interpolation between the point closest to the wall and the first point in the axial slice with a reliable measurement. The second strategy consists of using the closest reliable points in the axial and radial directions, weighted by distance, to extrapolate the value of the plasma potential to the unreliable point. The information contained in the uniform grid of LIF measurements is then interpolated onto the magnetic-field-aligned mesh of Hall2De by use of bilinear interpolation.

B. Two-dimensional plasma potential contours of the acceleration region

The two-dimensional maps of the ion velocity and plasma potential obtained from LIF measurements have been used in the Hall2De simulations in two ways. Starting from a Hall2De solution that exhibits good agreement with the LIF measurements along the channel centerline, in the first approach we superimpose the plasma potential obtained from LIF in the acceleration region. In other regions of the thruster where LIF measurements do not exist, the solution from the simulation is used. We allow ions to evolve according to the experimental plasma potential. The electron temperature equation contains an Ohmic heating term that depends on the electric field, which is also computed using the experimental information. In the second approach, we prescribe directly the measured ion velocity by assigning it to fluid 1 in our multi-fluid simulation (high-energy population). In regions of the computational domain where there are no measurements, the ion velocity is allowed to evolve according to the ion momentum equation. This approach does not produce discontinuities in the velocity field because the experimental velocity field is prescribed also as the boundary condition for the solution upstream and downstream of the acceleration region. The purpose of using these two different methods is to verify that the ion velocity indeed evolves according to the plasma potential and to identify possible limitations of the multi-fluid algorithm in the acceleration region, which typically defines the transition between the collisional plasma of the ionization region and the collisionless plasma of the plume region [20]. We work with five different scenarios in this subsection: the Hall2De solution with no experimental input, and the solutions using the first and second extrapolation methods for the plasma potential (termed shielded extrapolation and nearest extrapolation hereinafter, respectively). For each of the last two plasma potential solution, we conduct simulations with and without fixing the ion velocity field in the acceleration region.

In Fig. 5, we show contour plots of the plasma potential for the initial Hall2De solution and the solutions that make use of the experimental plasma potential with the two extrapolation strategies described above. Comparing this contour plots with those of the H6MS (Fig. 1), it is once again evident that the acceleration region at this operating condition of HERMeS is upstream of that of the H6MS and based on our discussion in Sec. II , the expected erosion rates at the poles for HERMeS were expected to be lower than for the H6MS. However, we find this is not the case. A first comparison between the Hall2De solution and the plasma potential extracted from LIF reveals the following differences. The plasma potential contours in the Hall2De solution exhibit a concave shape with axis at the channel centerline that is reflective of isothermality along magnetic field lines. In the direction parallel to the magnetic field, the pressure gradient is dominant over the resistive transport and Ohm's law can be approximated as

$$0 = -n_0 e E_{//} - \nabla_{//}(n_0 e T_e) - n_0 m_e \left((\nu_{ei}+\nu_{en})u_{e//} - \nu_{ei} u_{i//}\right) \approx= -n_0 e E_{//} - \nabla_{//}(n_0 e T_e), \quad (4)$$

and, thus, along magnetic field lines

$$\phi = \phi_{CL} + T_e \log\left(\frac{n_0}{n_{0CL}}\right), \quad (5)$$

where $\phi_{CL}$and $n_{0CL}$are the plasma potential and density, respectively, at the channel centerline. Thus, since the dependence on the density ratio is only logarithmic, plasma potential contours do not exactly follow magnetic field contours but closely resemble them. As a consequence of the shape of the magnetic field, we observe that, of the two lobes (highlighted by circles in Fig. 5) of the plasma potential contours near the outer and inner channel chamfers, the one near the outer chamfer extends further downstream than the one near the inner chamfer. In the measurements, however, the plasma potential contours appear to not follow the magnetic field lines as closely as in the simulation and the contours are aligned with the radial axis except at the chamfered regions of the channel. In these regions, we observe that the contours are approximately perpendicular to the walls. Here, the reader is reminded that it is nearest

to these chamfered walls that the LIF measurements were either unreliable or not available. The solution with the shielded strategy stops that trend close to the walls of the chamfered region while the nearest extrapolation strategy solution allows the plasma potential contours to intersect the walls. The implications of these differences between extrapolation strategies will be analyzed in detail in the next paragraph. Here we close by pointing out that, based on the comparisons of Fig. 5, the LIF-derived plasma potential contours seem to exhibit deviations from the computed contours which (as discussed above) assume that Eq. (5) is valid. This, in turn, suggests that deviations from Boltzmann's law do occur, at least in the acceleration region. One immediate consequence of such deviations would be, for example, that the lines of force are no longer isothermal in this region of the thruster. As we will show later in this article however, neither of the two experimentally-derived distributions nor the Hall2De solution can explain the observed pole cover erosion at the 300-V operating condition. Moreover, since deviations from Boltzmann's law diminish as the anode is approached, magnetic shielding of the channel will not be affected as it depends largely on the conditions deep in the channel interior. Hence, detailed investigations of deviations from Boltzmann's law are reserved for a separate study and are considered beyond the scope of the work reported in this article.

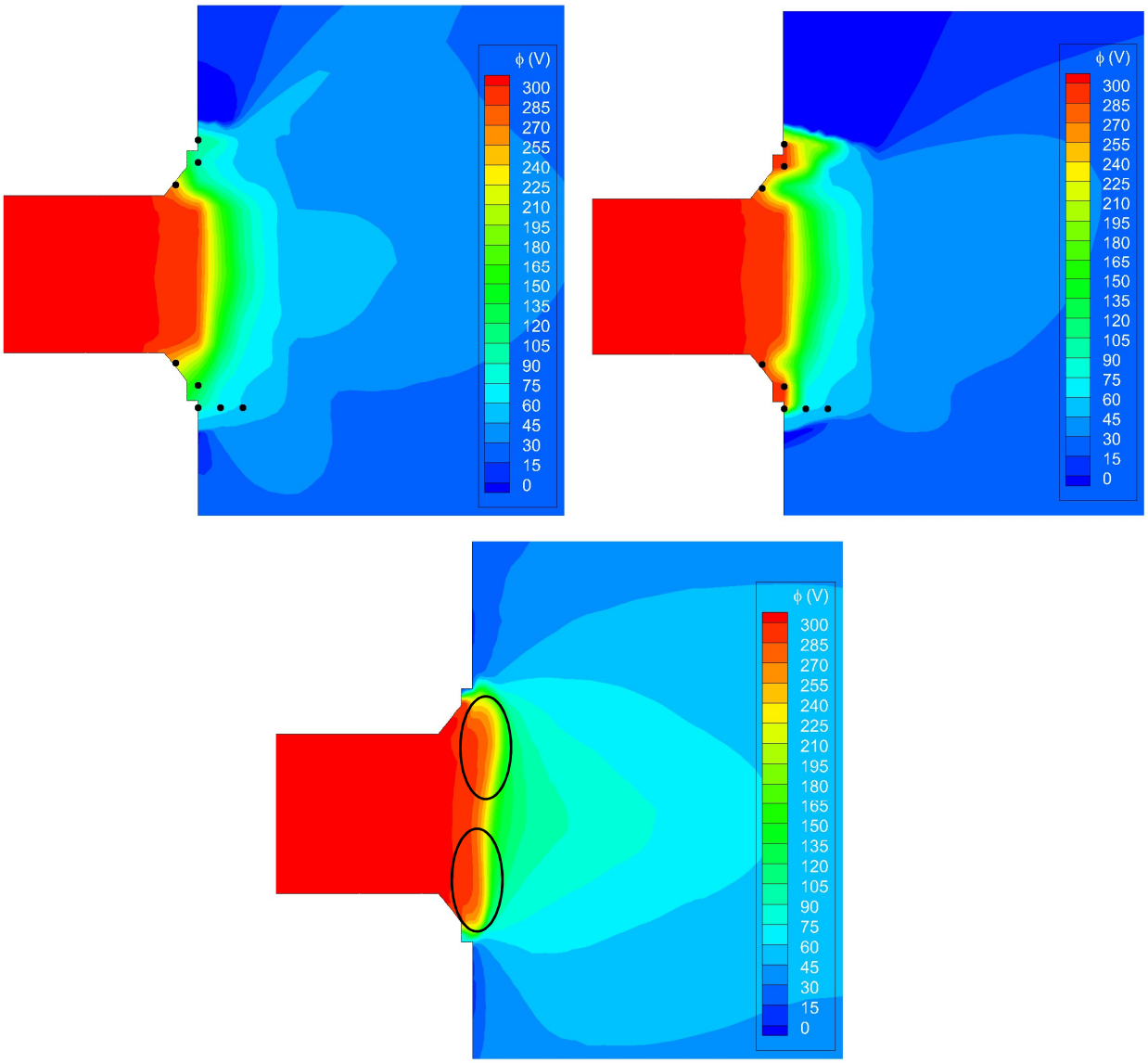

Figure 5. Plasma potential contours with LIF solution and nearest extrapolation strategy for unreliable points (left), shielded extrapolation strategy (right), and Hall2De solution with good agreement with LIF measurements at the channel centerline (bottom). Unreliable LIF measurements points are highlighted in black.

Figures 6 through 10 show the plasma potential contours, ion density and trajectories of high energy ions (above 270 V) for the five simulations considered in this article. We first comment on the differences observed between the simulations with and without a fixed ion velocity field in the acceleration region. Comparing Figs. 6 and 7, we observe that in the acceleration region the trajectories are similar for most of the channel width. At the chamfered regions, significant differences in the trajectories arise. At the outer wall, the measured trajectories diverge from an approximately 45-degree angle to being almost parallel to the outer pole cover surface. This change in direction occurs without the existence at that location of a plasma potential gradient that could justify it. The likely explanation for this phenomenon is depicted by the orange and magenta arrows superimposed in the figure. The ions that are generated close to the walls follow the magenta trajectory while the ions generated further from the wall follow the orange trajectory. The ions are found to be collisionless here and the trajectories are not perturbed. Thus, LIF measurements first measure the ions following the magenta trajectory and further away from the centerline measure the ions that follow the orange trajectory, given the impression of a change in trajectory. Because these ions are not treated as separate populations, our fluid formulation does not capture the fact that these distinct populations can cross paths. For the simulation in which the measured velocity field is specified directly and held fixed, the density is deflected radially with the apparent change in direction of the ions, resulting in higher ion density at the outer pole. For the simulation in which the velocity field is computed according to the Hall2De equations and the LIF-derived plasma potential, the ions in the magenta and orange trajectories actually collide, resulting in a plume of high density at an intermediate angle between the orange and magenta trajectories. With respect to erosion predictions, the fixed ion velocity solution (Fig. 6) likely over-predicts the erosion as it directs both the ions in the orange and magenta trajectories towards the outer pole. The free velocity solution under-predicts the erosion as it does not allow for the ions in the magenta trajectory to reach the vicinity of the pole. Indeed, the region in the vicinity of the outer pole surface appears to be void of high energy ions in Fig. 7. To properly account for the distinct populations and their trajectories, it would be necessary to establish a boundary in the simulation in which the fluid equations transition to a PIC formulation while conserving mass and momentum. We plan to incorporate this approach in Hall2De sometime in the future. With respect to the inner chamfered region, the major difference that we observe between Figs. 6 and 7 has to do with the fact that, in the simulation with fixed ion velocity, the ion trajectories are not perpendicular to the potential contours. From Eq. (3), the plasma potential is independent of the ion velocity and, thus, a proof that the ion trajectories are determined solely by the electrostatic force is that when the plasma potential is reconstructed from the ion velocity, the trajectories are perpendicular to the plasma potential contours. Possible explanations for the latter phenomenon are: the existence of an anomalous force, local plasma oscillations, or simply, insufficient resolution in the spacing of the LIF measurements. To address these concerns, an additional LIF campaign will be conducted involving increased resolution of the 2-D map and time-resolved measurements that can detect local oscillations. It is also worth pointing out here that the distinctively different behavior of the ion velocity field shown in Fig. 6, between the inner and outer near-chamfer regions, is not immediately clear especially in light of the observation that in the inner region the trajectories there do not seem to follow the electric field. Moreover, looking closely at the potential contours near the outer chamfer, it appears that only small changes in the potential near the inner chamfer would be required to produce the same ion velocity field as that near the outer chamfer. It is therefore possible that the details of the ion divergence, and in turn, the erosion of the poles, are highly sensitive to small changes in the potential structure near the chamfers. This would make it extremely challenging to capture by numerical simulation and/or by plasma diagnostics.

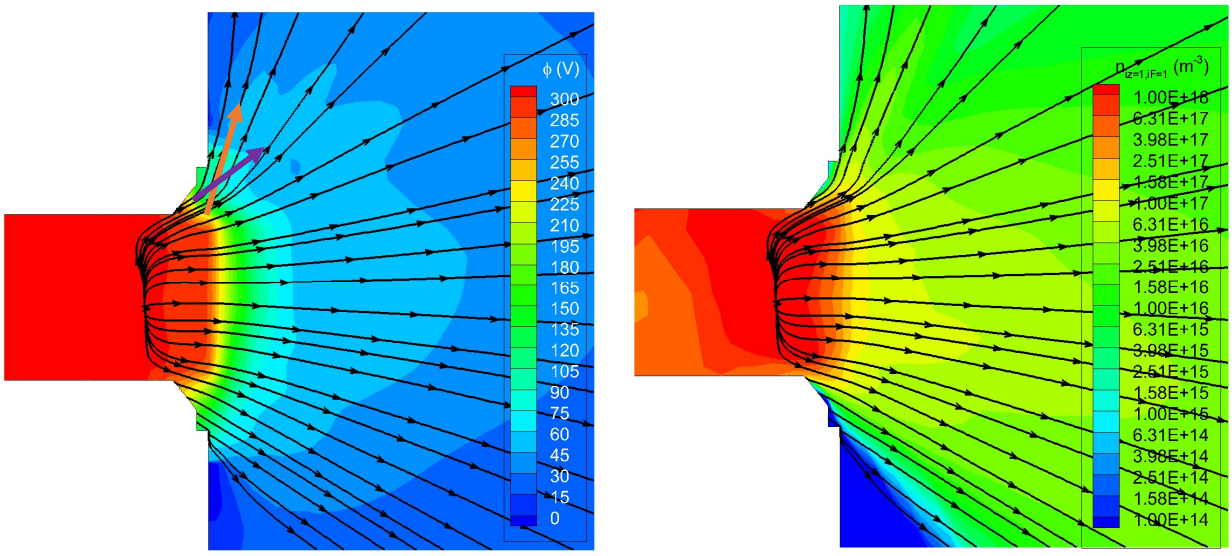

Figure 6. Contours of plasma potential and density of high energy singly-charged ions superimposed to ion streamtraces for the simulation with superimposed plasma potential with nearest extrapolation and fixed ion velocity in the acceleration region

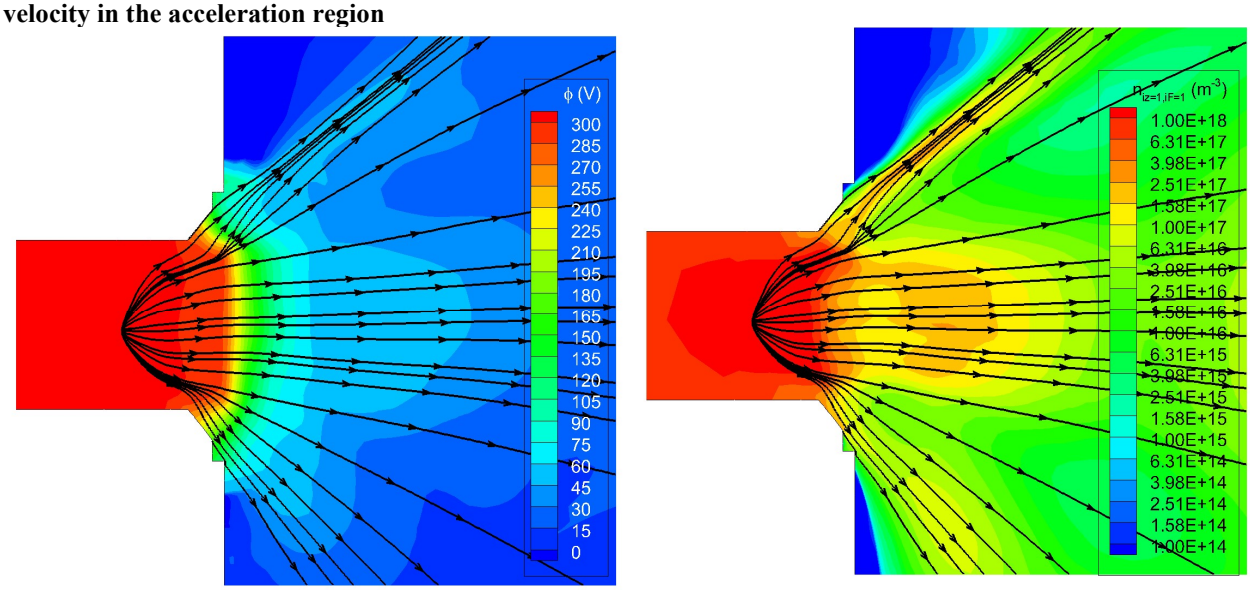

Figure 7. Contours of plasma potential and density of high energy singly-charged ions superimposed to ion streamtraces for the simulation with superimposed plasma potential with nearest extrapolation and free ion velocity in the acceleration region

A comparison between Figs. 8 and 9 (shielded extrapolation plasma potential) reveals the same conclusions already outlined for the solution with nearest extrapolation (Figs. 6 and 7) in the region in which the two plasma potentials are the same. For the gap between the chamfered region and the pole surface, we observe a large influence of our assumption of a 300-V potential. Examining Fig. 8 (fixed velocity), we conclude that this extrapolation strategy is not likely accurate between the pole and the channel as the ion trajectories are essentially unperturbed by the plasma potential. In Fig. 9, the ion velocity is free to evolve according to the prescribed plasma potential and we observe that the effect of the 300-V regions in between the channel and the poles is to narrow the beam, reducing its divergence. We can thus conclude that in reality the plasma will not include the region of 300-V potential at the channel-pole gap but, based on the examination of the magnetic field lines, can still consist of a narrow region of high potential in the chamfered region that assures magnetic shielding of the walls, a solution in between the two extrapolation strategies used in this article.

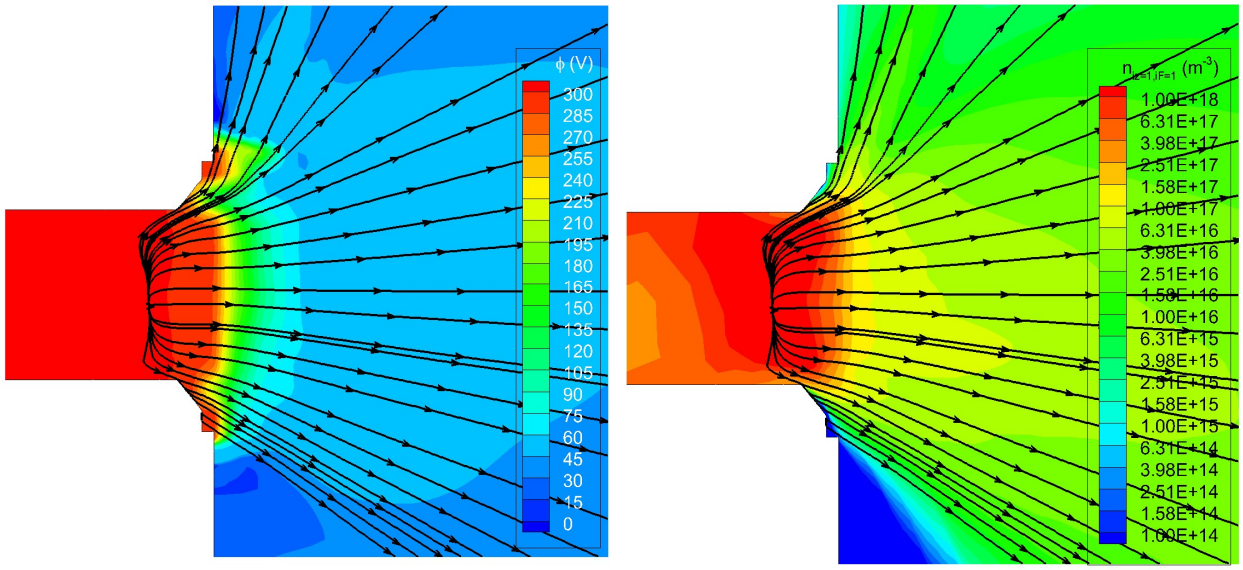

Figure 8. Contours of plasma potential and density of high energy singly-charged ions superimposed to ion streamtraces for the simulation with superimposed plasma potential with shielded extrapolation and fixed ion velocity in the acceleration region

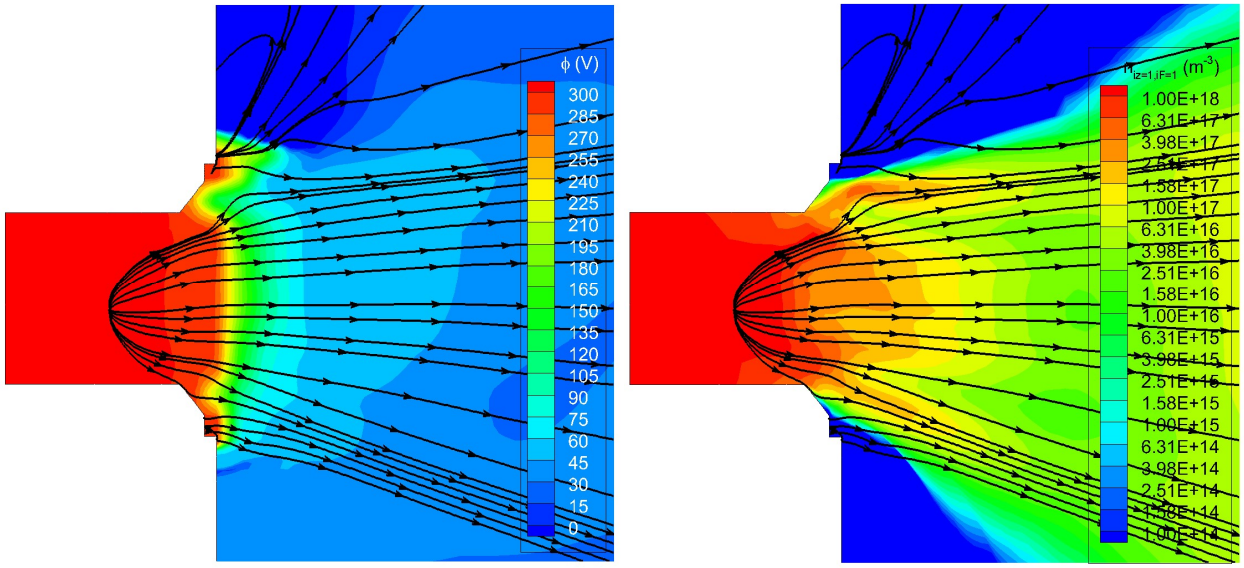

Figure 9. Contours of plasma potential and density of high energy singly-charged ions superimposed to ion streamtraces for the simulation with superimposed plasma potential with shielded extrapolation and free ion velocity in the acceleration region

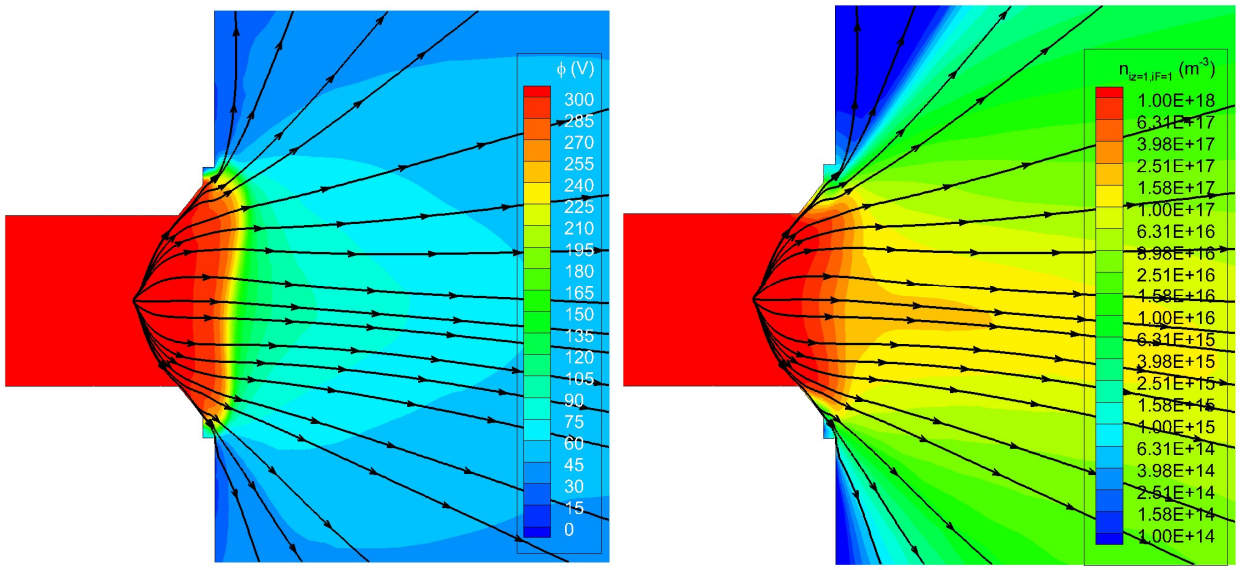

Figure 10. Contours of plasma potential (left) and density of high energy singly-charged ions (right) superimposed to computed ion streamtraces from the Hall2De simulation.

We also contrast the Hall2De solution (Fig. 10) with the solutions produced with the experimentally inferred plasma potential. In the initial Hall2De solution, the high potential contours extend futher into the chamfered region of the channel and acceleration of the ions at the edges of the beam occurs further downstream. However, we observe that the angle of the ions at the edges of the beam are similar to those found in the solution with free velocity and nearest extrapolation (Fig. 6). It is worth noting that none of these cases predict a significant amount of high energy ions in the vicinity of the inner pole and only one case (Fig. 7, nearest extrapolation with fixed velocity field) predicts a flux of high energy ions to the outer pole region. This is because the plasma potential does not establish the spatial distribution necessary to accelerate high energy ions radially, towards the poles (similarly for example to the distribution found in the H6MS, Fig 1). Since ions generated in the ionization region mostly follow straight lines from the point their acceleration begins (a result of the contour lines being close to each other in the acceleration region), the only plasma potential topology that can direct ions to the poles is one that has high potential contour lines parallel to the channel centerline (see, for instance, Fig. 1 for the H6MS). The high potential contour lines in Figs. 6-10 are either perpendicular to the channel centerline or at an angle. Only in Fig. 10, there are high potential contour lines that are parallel to the centerline but their location is upstream of the pole surface, which in turn results in ions sputtering the lateral surface of the pole but not the pole surface parallel to the channel exit. The accleration of ions at an angle at the edges of the beam results in only the outer edge of the inner pole and the inner edge of the outer pole being sputtered by a significant number of energetic ions. Along the surface, sputtering by high energy ions does not appear to be significant. This qualitative conclusions will be confirmed in next subsection, where we compute actual erosion rates.

A possibility that needs to be explored is whether less energetic ions (in the range of 100 to 250 V) can sputter the pole surfaces. This possibility is unlikely based on the results of a previous LIF campaign [17] that measured plasma potentials at operating conditions from 300 V to 600 V. It was found in this investigation that the plasma potential contours below 300 V were the same for all operating conditions. Thus, ions in the 100 to 250-V range would follow similar trajectories for all operating conditions and the sputtering at 300 V would be similar to that at 600 V. In contrast, erosion rates for wear tests predict higher erosion, by a factor of 2 to 3, at the 300 V condition. Figure 11 and 12 show the ion density and trajectories for ions whose energy range is 170 to 250 V and 120 to 170 V, respectively, in the simulation with nearest extrapolation and free velocity. The trajectories of these ions are similar to those found for more energetic ions because the plasma potential contours in the acceleration region are close together. We do not find that a significant amount of these ions populations sputter the poles. In Fig. 12, we observe a region of high density at the pole surface. This is because we are limited to using 3 distinct fluids in our multi-fluid simulations and had to combine in one fluid ions in the 120 to 170-V range with cathode ions. The high density region at the pole surface corresponds then to low-energy cathode ions. Plume ions below 120 V were modeled by PIC.

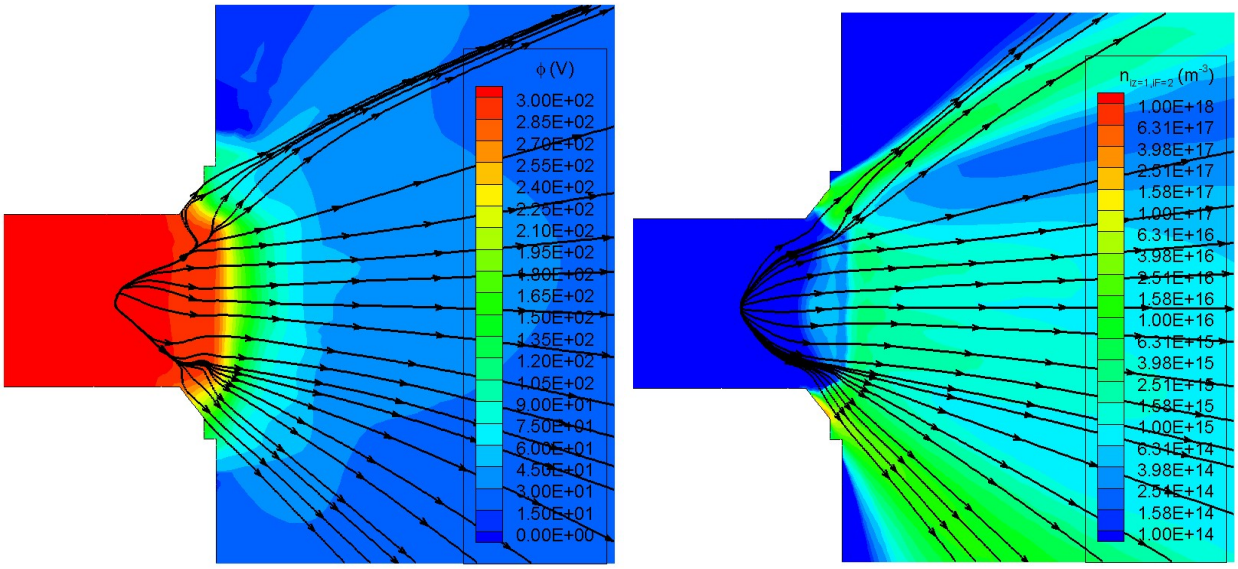

Figure 11. Plasma potential contours, ion density and trajectories for ions whose energy is between 170 V and 250 V for the simulation with superimposed plasma potential with nearest extrapolation and free ion velocity in the acceleration region

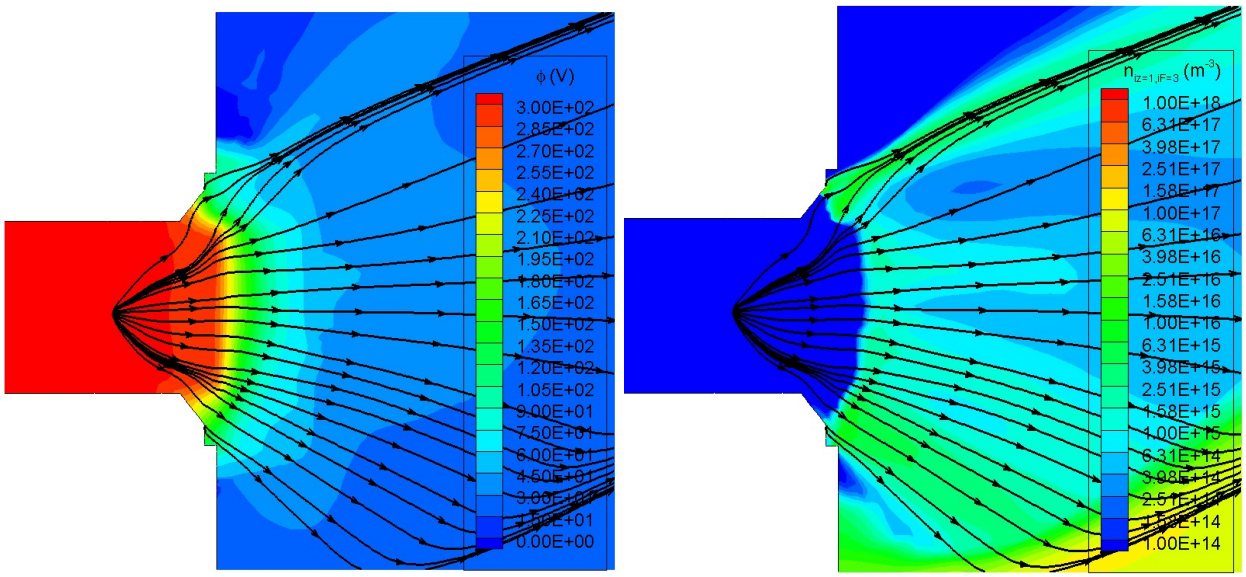

Figure 12. Plasma potential contours, ion density and trajectories for ions whose energy is between 120 V and 170 V for the simulation with superimposed plasma potential with nearest extrapolation and free ion velocity in the acceleration region

C. Erosion assessments

Figure 13 depicts the erosion rates at the inner and outer pole surfaces for the five simulations presented in the previous subsection. The carbon sputtering model described in [10] is assumed. We also show the measured erosion rates for the first and second wear tests (background pressure of 5 μTorr and 10 μTorr, respectively). The LIF measurements used in our simulations were obtained with a background pressure of 10 μTorr. For the inner pole, none of the simulations agree well with the measured erosion rates for the entire pole surface, which was expected based on our qualitative discussion in the previous subsection. The Hall2De initial solution exhibits the closest agreement to the measurement but it is still approximately an order of magnitude below the measured erosion for most of the pole surface. The reason for the Hall2De initial solution having a higher erosion rate is because plasma potential values in the plume are higher for this simulation than for the simulations in which the plasma potential solution were

superimposed, making the sheath potential at the pole surface also larger (e.g. compare potentials downstream of the acceleration region between Fig. 6 and 10). Most of the erosion computed for the Hall2De initial solution is due to PIC ions with energies below 120 V. These ions increase their sputtering rate when they experience a larger sheath potential at the pole surface. In the superimposed solutions, the plasma potential outside of the region measured by LIF is still self-consistently computed but evolves based on the current, temperature and plasma density distributions obtained when assuming an experimental solution for the plasma potential in the acceleration region, leading to changes in the plume plasma potential values. The conclusion is similar to that found in [16]: low energy ions account for, at most, 10% of the erosion rates measured at the inner pole. This statement is also backed by the LIF measurements conducted by Huang, et al. [19] in the proximity of the inner pole. The measurements showed that the main ion population had an average energy in the range of 3 to 12 V (depending on the location). Even though these measurements were made outside of the sheath and the ions can gain additional energy, the reported values are well below the sputtering threshold of graphite. The only region in which the sputtering rates are larger than measured for some of the simulations run (especially for the simulations with the nearest extrapolation strategy) is the outer edge of the pole. The sputtering here is produced by high energy ions of energies above 120 V (as shown by Fig. 7, 11 and 12) but because the trajectories of these ions are not radial, they only affect a small portion of the pole surface.

For the outer pole, we do not have measurements of erosion rates on graphite at the nominal magnetic field. We use instead the erosion rates measured at 75% and 125% of the nominal magnetic field to provide an approximation to what the actual erosion rate might be at the nominal magnetic setting. In this case, we observe that the initial Hall2De solution and the solutions with fixed velocity in the acceleration region predict values of the erosion that are close to the measurements. We already discussed in the previous subsection that the cases with fixed velocity displaced the ions into the outer pole due to the curved ion trajectory at the outer chamfered region. We also argued that this effect was likely over-estimated because in reality the ions directed to the poles (orange arrow in Fig. 6) cross over ions that are not directed to the pole (magenta arrow in Fig. 6). The fluid algorithm convects all these ions into the pole region. In the simulations with free velocity field, the topology of the plasma potential does not accelerate energetic ions in the radial direction. As described in the previous subsection, the ions in the magenta and orange flows collide when ions are modeled as fluid, with the fluid solution being in between the two trajectories and at an angle to the pole surface. For the initial Hall2De solution, we observe that high-energy ions above 250 V are directed at an angle and do not cause erosion of the outer pole. In this case, it is slightly less energetic ions (in the range of 120 V to 270 V) that produce the erosion. The reason for which this phenomenon is not also observed in the inner pole is as follows. The plasma potential contours in the initial Hall2De solution follow more closely magnetic field lines than the measured profiles. This results in a sinusoidal structure of the plasma potential that was already discussed in the last subsection. The lobe closest to the outer wall is more downstream that the lobe closest to the inner wall (Fig. 5), which in turn means that when the plasma potential contours turn in the chamfered region, there exist high energy contour lines parallel to the centerline and that slightly extend downstream of the pole surface. The latter allows a small ion current of ions that have been generated slightly downstream of the ionization region to be accelerated in the radial direction. The inner lobe is more upstream so the high energy contour lines parallel to the centerline are not downstream of the pole surface and ions are not accelerated radially towards the pole surface. It is worth noting that the current density of energetic ions necessary to account for the measured erosion at the outer pole is very small. We find values in our simulations that range from 1 to 10 A/m^2. These values are approximately 60 to 600 times smaller than the ion current density in the axial direction at the center of channel. Finally, we also point out that the measured erosion rates at the inner edge of the outer pole are, similarly to what was observed at the outer edge of the inner pole, larger than the measurements. The significance of this will be discussed in the next section.

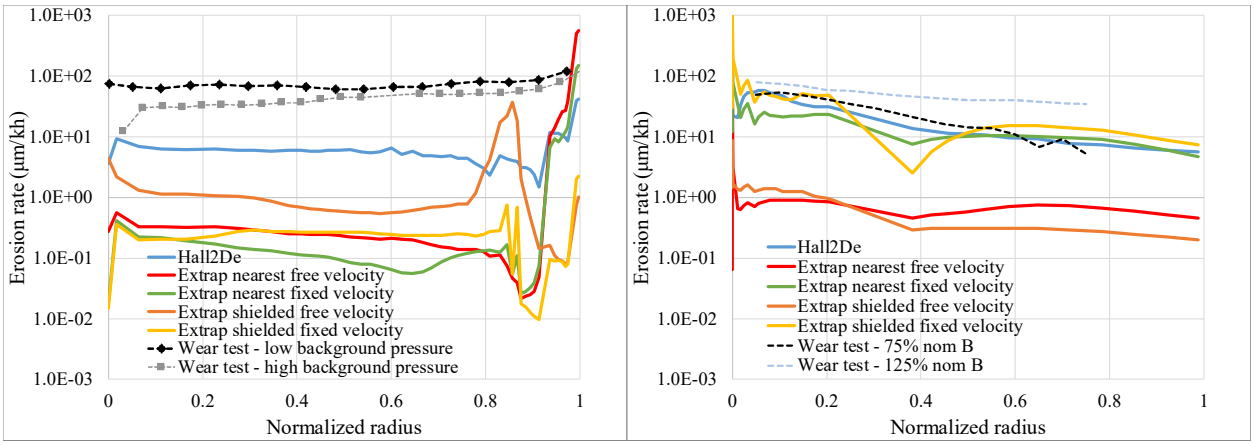

Figure 13. Computed erosion rates at the inner pole surface (left) and outer pole surface (right)

V. Proposed mechanisms that can lead to increased erosion rates at the pole surfaces

At the end of section II, we cited three possible causes that could explain the disagreement found between computed and measured erosion rates for HERMeS at 300 V – 20.8 A and nominal magnetic field in [10]: uncertainty in erosion measurements, uncertainty in LIF measurements, and sensitivity of the erosion rates to the off-centerline plasma potential contours. The first two possibilities were addressed by additional measurements that did not produce an outcome that was significantly different from the original results. Section IV of this article was devoted to investigating the sensitivity of the erosion rates to the off-centerline plasma profile. We were able to determine that none of the scenarios predicted values of the erosion rate at the inner pole cover that were close to the measurements for the entire surface, even though the off-centerline profiles from the measurements were different from the Hall2De solution. In this section, we explore possible erosion-enhancing mechanisms not currently incorporated as models in Hall2De, elaborate on their likelihood using simplified calculations, and propose further measurements that can be made to confirm their presence in Hall thrusters.

A. Two-dimensional sheath effects at the outer edge of the inner pole and inner edge of outer pole

Here we revisit a previous hypothesis [26, 27] that sheaths formed near the downstream wall edges of the channel may be responsible for turning high-energy ions to divergence angles greater than those predicted by hydrodynamic quasi-neutral models. We observe from the contour plots of the ion density (for instance, in Fig. 7) that at the outer edge of the inner pole, the ion density is relatively large but, since the ion beam trajectory is not perturbed by the presence of the corner, an area of low density develops downstream of the corner. The existence of a low density region next to the pole surface is also captured in LIF measurements. In Fig. 4, there are three points at the first horizontal row of measurements (starting from the inner pole) for which measurements are unreliable. At these points, the signal-to-noise ratio was small, meaning that the ion density in those locations was low enough that the optics equipment could not capture any significant signal of ion excitation. It is well known that there exists a sheath next to the walls and that the quasi-neutrality assumption for ions and electrons breaks down in this sheath. The thickness of the sheath is given by the Debye length,

$$\lambda_{De} = \sqrt{\frac{\varepsilon_0 T_e}{e n_0}}. \tag{6}$$

In Hall2De, we assume that the sheath is infinitesimally small and its effect is captured in the form of a boundary condition [27] for ion velocity, electron current and thermal fluxes. In the case of a finite sheath (Debye length larger than the cell width in Hall2De), the space-charge algorithm outlined in [12] is employed. The Debye length at the outer edge of the inner pole (see Table I) is approximately 0.4 mm and half the width of a cell in this region. Thus, modeling the sheath at the outer edge of the inner pole is challenging because the width of the sheath is large for the infinitesimally small assumption and small for the space-charge algorithm to affect the plasma potential field. Using a fluid dynamics analogy, the corner resembles a location from which an expansion fan would develop in a highly resolved fluid dynamics simulation. This configuration will also lead to an abrupt increase in the width of the boundary layer (the equivalent of the sheath), downstream of the corner.

We extend here the argument made previously by the authors [27] that some of the high energy ions in the beam whose trajectories come close to the outer edge corner of the inner pole get trapped in the sheath as the width of the sheath increases immediately downstream of the corner (Fig. 14, left). The same argument is made for the inner edge of the outer pole. As shown in Table I, the plasma potential at the corner is approximately 110 V. Here we assume that the pole cover surface is a graphite conductor biased at 0 V. Thus, the ions in the sheath experience a 110 V change in potential within the sheath. In reality, the voltage of the surface is coupled to the cathode potential but this would modify the potential drop in the sheath by approximately only 10 V. We can compute an estimate of the ion current that gets trapped in the sheath using

$$J_{i,sheat\ ,inner} = en_0 u_i 2\pi\lambda_{De} r_o. \quad (7)$$

This quantity is computed from the local plasma parameters at the outer edge of the inner pole. For simplicity, we have assumed that the population of high energy ions is dominant at the outer edge of the inner pole and, thus, $n_{iZ=1,iF=1} \sim n_0$. The latter is supported by the results in our simulations.We now assume that all the ions trapped in the sheath end up sputtering the pole surface, the average ion current density onto the inner pole surface is

$$j_{i,avg,inner} = en_0 u_{ir} \frac{2\lambda_{De} r_o}{(r_0^2 - r_i^2)}, \quad (8)$$

where u_{ir} in this case is the ion velocity in the radial direction. Conversely, for the outer pole

$$j_{i,avg,outer} = en_0 u_{ir} \frac{2\lambda_{De} r_i}{(r_0^2 - r_i^2)}. \quad (9)$$

The energy of the ions sputtering the walls is the sum of the energy they had at the corner where they entered the sheath and the potential drop in the sheath. The average erosion rate is computed as

$$\dot{\varepsilon_r} = j_{i,avg} Y(\varepsilon_i + \phi_{sheat}\ )\beta, \quad (10)$$

with $\varepsilon_i = \frac{m_i u_i^2}{2e}$ the kinetic energy at the corner and β the angular yield. In Tables I and II, we give values for these quantities for three of the cases explored in the previous section. The cases with shielded extrapolation were not considered as we discussed in the previous section that the 300-V contours in the gap between channel walls and poles did not appear to be realistic. We assume that β=1. The latter is likely an under-estimation since the ions have

significant radial velocity and are likely to sputter the surface at an angle. Our angular yield models [10, 12] predict that β can be close to 3 at high incidence angles.

Table I. Plasma parameters at outer edge of inner pole and erosion estimate from Eq. (8, 10)

INNER POLE	Initial Hall2De	Nearest extrapolation – fixed ion velocity	Nearest extrapolation – free ion velocity
n_0 (m^{-3})	1.25x10^{16}	3.83x10^{16}	1.42x10^{17}
λ_{De} (m)	4.14x10^{-4}	2.34x10^{-4}	1.23x10^{-4}
ϕ_{sheath} (V)	113.0	111.2	111.7
ε_i (eV)	136.5	145.3	151.2
ε_{iz} (eV)	34.8	55.8	59.5
$j_{i,avg}$ (A/m^2)	0.38	0.68	1.34
Y(mm^3/C)	4.03x10^{-3}	4.25x10^{-3}	4.44x10^{-3}
$\dot{\varepsilon}_r$(μm/kh) (β=1)	5.52	10.4	21.5

From Table I, we observe that the current density (evenly averaged over the surface of the pole) increases with the plasma density at the outer edge of the inner pole, as Eq. (7) scales with $\sqrt{n_0 T_e}$. The sheath potential drop is similar for all three cases. The total energy of the ions when reaching the walls is the sum of ε_i and ϕ_{sheath} and approximately 250 V. For obtaining ε_i, we averaged the velocity over all the fluid populations (*iF*) in the simulation. The computed erosion rates are between 5.52 and 21.5 μm/kh, depending on the case. The average erosion rate from wear tests is approximately 60 μm/kh. Our estimates are then below the measurement or comparable to the measurement in the most optimistic case if we assume that β is close to 3. Assuming β=1, the estimated erosion due to sheath effects is comparable to (in the worst case) and higher by a factor of 4 (in the best case) than the predictions of our simulations shown in Fig. 13. The estimated values can be underestimations due to the choice of β=1 but also be overestimations because we assume that all the ions that enter the sheath at the corner end up sputtering the pole cover surface. To confirm that a significant portion of the ions do not escape the sheath downstream, we provide in Table I values of the axial velocity of the ions (i.e., velocity in the direction opposite to the wall) in units of energy. The computed values range from 35 V to 60 V and can be overcome by the potential drop (approximately 110 V) that occurs within the sheath. In Fig. 14, we plot the plasma potential immediately outside of the sheath and the Debye length along the surface of the inner pole. We observe that the potential outside the sheath falls very rapidly from 110 V to 30 V within the 20% of the pole surface closest to the outer edge. In this region, the sheath width does not change significantly (i.e., the decrease in plasma density is compensated by a similar decrease in electron temperature in Eq. (6)). If the sheath width decreased rapidly downstream of the corner, we should expect that a significant fraction of the ions can escape the sheath as they would still have significant axial velocity but this is not the case here. We expect instead that similarly to what happens with the exterior plasma potential, a substantial drop in the plasma potential occurs in the sheath immediately downstream of the corner, preventing the ions from escaping and directing them towards the walls. This hypothesis must be of course confirmed by a more detailed theoretical or numerical analysis.

Using simplified estimates we have argued that two-dimensional sheath effects at the corner of the outer edge of the inner pole can explain a significant part of the erosion observed at the inner pole. In order to gain confidence on the viability of this hypothesis, we apply it now to the outer pole of the thruster. In Table II, we present estimates of the erosion rates due to two-dimensional sheath effects at the inner edge corner of the outer pole. We obtain in all three cases lower erosion rates that those estimated for the inner pole. The reasons are that the electron temperature is lower at the corner of the outer pole, decreasing the sheath width and in turn the current of ions into the sheath, and that at the outer pole the ion flow naturally expands because ions move radially outwards while at the inner pole the flow moves inwards radially (i.e., at the inner pole, $\frac{2\lambda_{De} r_o}{(r_0^2 - r_i^2)}$ is the ratio between the current into the sheath and how the current is being distributed evenly at the surface of the pole, with $r_0 > r_i$, at the outer pole the same ratio takes the form $\frac{2\lambda_{De} r_i}{(r_0^2 - r_i^2)}$ instead). It is worth noting that at the outer pole, it is also likely that most of the trapped ions stay in the

sheath because the width of the sheath increases immediately downstream of the corner and this increase is accompanied by a rapid decrease of the plasma potential outside. The axial velocity is also lower than the sheath potential except in the case with nearest extrapolation and free ion velocity. We discussed in the last section that the solution for the latter case at the outer edge of the beam was probably not accurate because the trajectories were influenced by ions moving in converging directions resulting in collisions when modeled as a fluid while the trajectories obtained directly from the velocity measured by LIF suggested that the ions moving in converging directions could cross their paths without colliding. The measured erosion rates at the outer pole (estimated from the operating conditions at 75% and 125% of the nominal magnetic field since no measurements are available for the nominal condition) are on average 40 μm/kh, with higher values reported next to the inner edge. Our estimates in Table II fall short of the average erosion rate by a factor of 5 even when assuming β=3. However, as seen in Fig. 13, some of our simulations produce erosion rate estimates close to those measured without including the effect of the sheath at the corner. This is because for these simulations, there exist ion trajectories towards the outer pole surface without the need of entrapment by the sheath. In particular, the simulation with nearest interpolation and fixed ion velocity captures the measured velocity field and at the same time, predicts the erosion rates at the outer pole. Further confirmation of the fact that the sheath effect may not be as important at the outer pole comes from the LIF measurements. In Fig. 4, we observe that, while at first horizontal row of measurements (starting from the inner pole) there were three points for which measurements were unreliable due to small signals, at the last row, only the closest point to the wall is unreliable, suggesting a less wide sheath at the outer pole. In addition, Huang et al. conducted measurements in the vicinity of the outer pole at distances of 0.025L, 0.075L to the surface that found ions with an average energy of 110-120 V in the region. High energy ions were likely not found in LIF measurements at the inner pole for two reasons: the amount of low energy ions in the inner pole region is much larger than at the outer pole,

making harder to distinguish a low-current density, high-energy population and/or the high energy ions were trapped in the sheath, whose width is less than the closest distance to the surface for which measurements were made.

Table II. Plasma parameters at inner edge of outer pole and erosion estimate from Eq. (9, 10)

OUTER POLE	Initial Hall2De	Nearest extrapolation – fixed ion velocity	Nearest extrapolation – free ion velocity
n_0 (m^{-3})	2.65x10^{16}	3.27x10^{16}	3.01x10^{15}
λ_{De} (m)	6.77x10^{-4}	1.87x10^{-4}	7.39x10^{-4}
ϕ_{sheath} (V)	85.2	98.5	98.5
ε_i (eV)	168.1	93.9	200.1
ε_{iz} (eV)	3.8	10.9	130.0
$j_{i,avg}$ (A/m^2)	0.11	0.27	0.15
Y(mm^3/C)	4.16x10^{-3}	2.42x10^{-3}	5.88x10^{-3}
$\dot{\varepsilon}_r$(mm/h) (β=1)	1.58	2.34	3.07

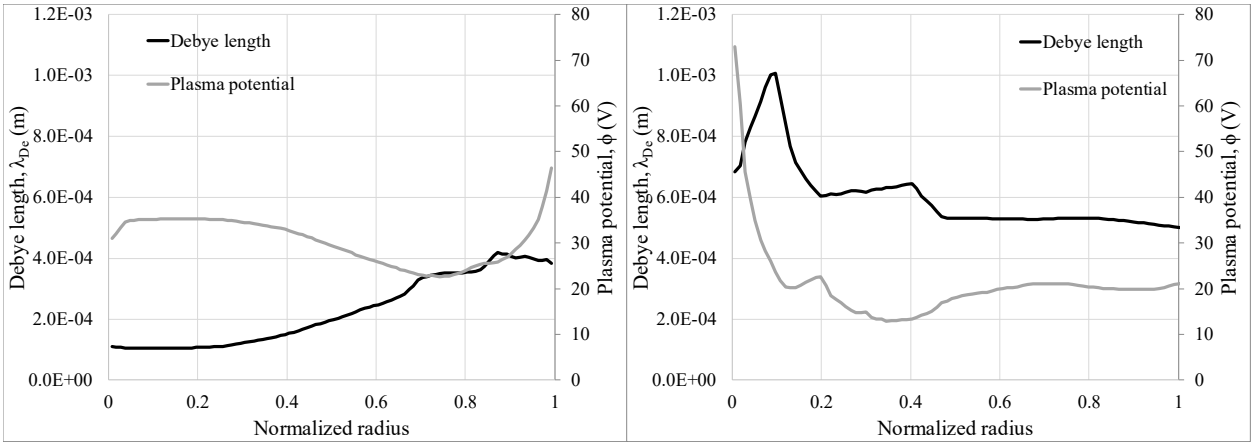

Figure 14. Debye length and plasma potential along the inner pole (left) and outer pole (right) surfaces from the initial Hall2De simulation

We must also discuss briefly here whether erosion being produced by high energy ions getting trapped in the sheath at the corner of the poles can account for the erosion rates found for different operating conditions and different thrusters. For the H6MS at 300 V – 20 A, we predicted erosion rates using Hall2De that were in agreement with the experiments [28]. Referring to the plasma potential contours for the H6MS (Fig. 1), we find that this case can have a similar explanation to the erosion rates at the outer pole of HERMeS at 300 V – 20.8 A: there exist plasma potential contours that drive the ions directly onto the inner pole surface. In fact, the streamtraces in Fig. 1 suggest that ions already have negative axial velocities when they reach the corner of the pole and, thus, a change in direction in the sheath does not occur. For the H6US and operating conditions for HERMeS in the 400 V to 600 V range, we observe that the divergence of the beam is lower than at 300 V because the location of maximum acceleration of the beam is located further upstream [10, 17] than in the 300-V case. A consequence of the latter is that the density of ions at the corner of the inner pole is lower (Fig. 15). Since the current density of sheath-trapped ions scales as $\sqrt{n_0 T_e}$, the contribution to the erosion by these ions decreases. Figure 15 then suggests that the erosion rates due to ion entrapment in the sheath should decrease with discharge voltage. Wear tests show similar erosion rates in the 400 V to 600 V

range because the presence of global large oscillations at 500 and 600 V, as shown in [10], overcome the decrease in erosion due to sheath effects.

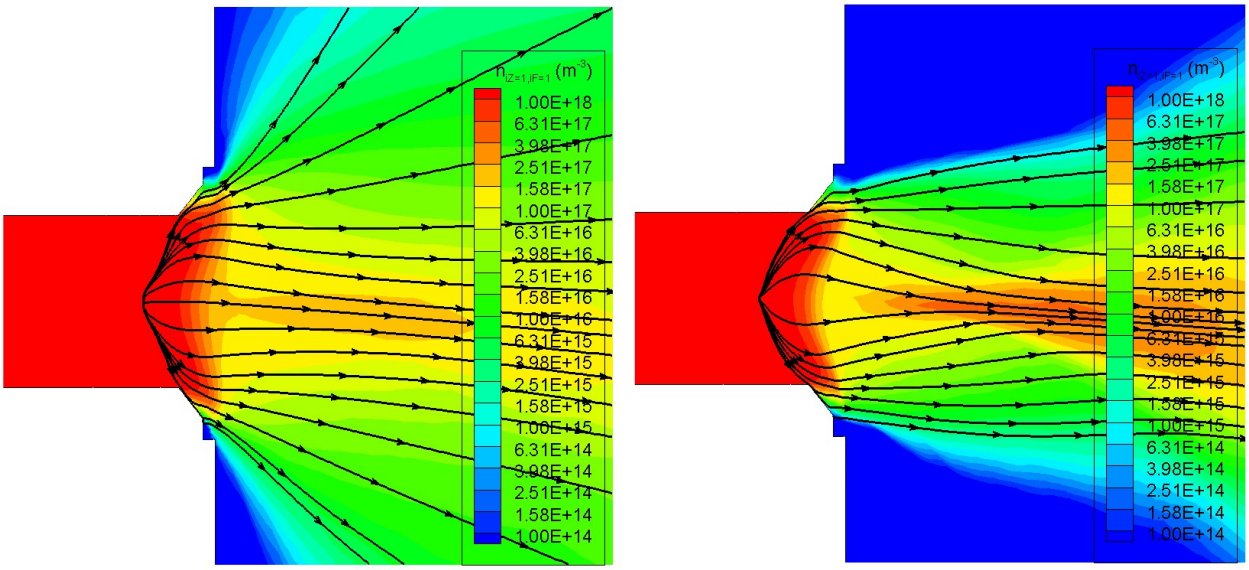

Figure 15. Density contours and trajectories of high energy ions from Hall2De simulations for HERMeS at 400 V – 20.8 A (left) and 600 V – 20.8 A (right) with nominal magnetic field. Compare density at the outer edge of the inner pole with Figs. 6-10.

B. Local oscillations in the vicinity of the gap between channel walls and poles

By contrast to the 600-V operating condition, we do not observe large-amplitude breathing-mode oscillations in HERMeS at 300 V – 20.8 A. As shown in [10], the amplitude of the oscillations in the discharge current was of approximately 11% of the nominal value. However, it is still possible that local oscillations that do not affect the global performance parameters may exist at the edges of the beam. One argument that supports this hypothesis is that the ion current density at the edge of the beam is approximately 10 to 100 times lower than at the centerline so any oscillation that perturbs the plasma between the channel walls and the poles may be considered a second order effect that is not visibly reflected in global measurements such as discharge current. Due to the low plasma density in the regions of interest, the presence of local oscillations may be coupled with sheath effects and have a direct connection to the hypothesis presented in subsection A. With the aim of understanding whether oscillations occur at the edges of the beam, an additional LIF campaign that includes time-resolved measurements will be conducted at JPL. The success of this campaign may be challenged though by the same low signal-to-ratio problems that the GRC campaign encountered for measurements in the vicinity of the outer edge of the inner pole and inner edge of the outer pole.

C. High energy ions in the cathode plume

The presence of high energy ions in the cathode plume is caused by the ion-acoustic turbulence that develops due to the relative drift between electrons and ions [13]. However, the magnitude of the instability and, in turn, the amount of energetic ions can be mitigated by operating the cathode in the appropriate range of discharge current and mass flow rate [14]. Generally speaking (more detail can be found in [14]), low discharge currents and large neutral mass flow rates lead to attenuation of the instability. The HERMeS cathode is operated at mass flow rates and discharge current conditions that should negate the presence of large ion-acoustic waves in the cathode plume. Our simulations with OrCa2D of the HERMeS cathode [29] actually found that the difference between the plasma potential in the plume and inside the cathode is relatively small, an indicator of low-amplitude ion-acoustic waves. Apart from the evidence gathered from our OrCa2D simulations, there are several arguments that can be made against the possibility of high energy ions from the plume causing significant erosion at the poles. First, the nominal operating envelope of HERMeS is at constant current of 20.8 A. The cathode operating conditions then should be almost identical at varying discharge voltage of the thruster because most of the potential drop occurs in the acceleration region of the thruster,

the current that the cathode must produce is the same, and the cathode mass flow rates are very similar. If a significant amount of high-energy ions were produced in the cathode plume, they should affect the erosion rates for all the operating conditions in approximately the same manner. However, we measured much higher erosion rates at the 300-V operating condition. The second argument against this hypothesis is that the erosion of the inner pole increases close to the outer edge. Since the density of cathode plume ions rapidly decreases away from the cathode, we would see higher erosion rates at the inner edge than at the outer edge of the inner pole if cathode ions had a significant effect on the erosion. To further evaluate the likelihood of this hypothesis, the JPL LIF campaign will include measurements of the ion velocity distribution function in the cathode plume for the thruster operating at 300 and 600 V with the objective of determining whether significant changes in the ion energy occur when operating the thruster at different conditions.

D. Sensitivity of the erosion rates and acceleration region to the experimental environment

In Fig.2 (right), we showed erosion rates for the inner pole at the 300 V and 20.8 A condition with nominal magnetic field for three different wear tests. The difference in measured erosion between the two wear tests run at lower background pressure (5 μTorr) is 30% in some locations but in most locations is within the experimental uncertainty. Erosion rates at the higher background pressure (10 μTorr) appear to be consistently lower than at the lower background pressure but they can also fall within the experimental uncertainty. These results can then suggest that the erosion rates are sensitive to the experimental environment. For instance, LIF measurements were performed at 10 μTorr but not at the same time as the wear tests in Fig. 2. Chaplin et al. [17] measured with LIF a downstream motion of the acceleration region of less than 5% of the channel length when decreasing the background pressure from 20 to 10 μTorr. LIF measurements have not been made below 10 μTorr so we cannot know if the observed trend continues for lower background pressures. However, if the acceleration region continues to move downstream from 10 to 5 μTorr, the physics in subsection A qualitatively predicts higher erosion rates at 5 μTorr because the divergence of the beam would increase and so would the density of ions at the outer edge of the inner pole. We also observe in Fig. 5 (left) that the differences between the plasma potential contours above and below the channel centerline are almost symmetric. However, the contours above the channel centerline accelerate some high-energy ions radially while the contours below the centerline do not. We can hypothesize that small changes in these contours (i.e., smaller than the spatial resolution of the LIF measurements) may occur between thruster runs or even as the thruster operation progresses and alter the current density of ions at the edges of the beam that are accelerated towards the poles.

In order to lower the uncertainty associated with the experimental environment, LIF measurements for background pressures below 10 μTorr will be made in the future. There are also plans to increase the spatial resolution of the LIF measurements at the edges of the beam in an upcoming campaign at JPL. The latter will capture with more precision the details of ion velocity field in the chamfered regions of the thruster and comparison with [19] may allow us to determine how much the solution changes for different runs of the thruster at the same operating condition. From the simulation standpoint, we may need to use sensitivity calculations to bound the erosion rates at vacuum conditions.

VI. Conclusion

Our past investigation of the erosion rates at the pole cover surfaces of HERMeS [10] predicted the measured erosion at 600 V and 20.8 A but yielded lower than measured values at 300 V and 20.8 A; the difference between numerical predictions and measurements was approximately an order of magnitude. At the lowest backpressure in which the thruster was operated, the measured erosion rates at 300 V were higher than in any other operating condition. Understanding the physical mechanisms that drive the erosion at 300 V is key to achieving the AEPS throughput requirements. Since previous Hall2De simulations have been capable of predicting accurate erosion rates at the poles for the H6MS, H6US and HERMeS at operating conditions other than 300 V, we identified three possible causes for the discrepancies observed at 300 V. The first two, uncertainty in the erosion measurements and LIF measurements in [10], were addressed with additional measurements that revealed no significant differences with the original results. The third possible cause was motivated by the disagreement observed between our simulations and the LIF measurements for a small number of locations away from the channel centerline, and was discussed in [10]. We determined that, since the erosion rates at the poles in thrusters such as the H6MS were driven by the plasma potential contours downstream of the channel exit and near the walls, small differences in the shape of these contours could lead to more ions sputtering the pole surfaces. Additional LIF measurements off-centerline were made to produce a

more complete 2-D map of the ion velocity and plasma potential in the acceleration region that could be compared with simulation results.

We examined the plasma potential contours extracted from LIF and compared them with those obtained directly from simulations. We found that none of the simulations that made use of the experimental plasma potential to compute ion trajectories predicted increased erosion rates at the poles. The location of maximum acceleration for the experimental plasma potential near the channel walls is upstream of the pole surface and ion trajectories only grace the corner of the outer edge of the inner pole but can never turn to sputter the surface. At the outer pole, some ions can actually be accelerated directly towards the poles (the profiles above and below the centerline are not exactly symmetric). Sputtering of the inner pole is then only driven by low energy ions whose energies are close to the sputtering threshold of graphite and cannot account for the measured erosion rates.

We concluded this article by proposing four different hypotheses that may explain the higher-than-predicted erosion at the pole covers. We argue that some high energy ions grazing the corner of the outer edge of the inner pole can become trapped by the local sheath. Then the electric field inside the sheath can turn the ions around the corner and into the pole cover surface. Simplified estimates of the trapped flux and energy of these ions suggest that the contribution to the erosion rate can be similar the measured erosion rates. We also proposed based only on qualitative arguments that (1) oscillations in the plasma, local to the downstream channel corners, and (2) high energy ions associated with the cathode plume, may also lead to increased erosion rates at the poles. We also argued that the experimental conditions for wear tests and during LIF measurements can have an influence on the erosion rates and the plasma potential contours in the chamfered regions of the channel. These hypotheses will be tested in the near future using a combination of LIF diagnostics and additional numerical simulations.

Acknowledgments

The authors would like to acknowledge Dr. Wensheng Huang and Dr. Vernon Chaplin for the obtaining the LIF measurements employed in this article and Dr. Jason Frieman, Dr. Peter Peterson, and Dr. Jim Gilland for conducting the wear tests and providing the erosion rate measurements. The research described in this paper was carried out by the Jet Propulsion Laboratory, California Institute of Technology, under a contract with the National Aeronautics and Space Administration. The support of the joint NASA GRC and JPL development of the Advanced Electric Propulsion System by NASA's Space Technology Mission Directorate through the Solar Electric Propulsion Technology Demonstration Mission project is gratefully acknowledged.

References

1. Hofer, R. R., Polk, J. E., Sekerak, M. J., Mikellides, I. G., Kamhawi, H., Sever-Verhey, T. R., Herman, D. A., and Williams, G., "The 12.5 kW Hall Effect Rocket with Magnetic Shielding (HERMeS) for the Asteroid Redirect Robotic Mission", AIAA paper 2016-4825, July 2016.
2. Herman, D., Tofil, T., Santiago, W., Kamhawi, H., Mcguire, M., Polk, J. E., Snyder, J. S., Hofer, R., Picha, F., Jackson, J., and Allen, M., "Overview of the Development and Mission Application of the Advanced Electric Propulsion System (AEPS)," IEPC-2017-284, October 2017.
3. Hofer, R. and Kamhawi, H., "Development Status of a 12.5 kW Hall Thruster for the Asteroid Redirect Robotic Mission," IEPC-2017-231, October 2017.
4. Williams, G., Gilland, J. H., Kamhawi, H., Choi, M., Peterson, P. Y., and Herman, D., "Wear Trends of the HERMeS Thruster as a Function of Throttle Point," IEPC-2017-207, October 2017.
5. Mikellides, I. G. , Katz, I., Hofer, R. R., Goebel, D. M., de Grys, K. H., and Mathers, A., "Magnetic Shielding of the Channel Walls in a Hall Plasma Accelerator," Physics of Plasmas, Vol. 18, no. 3, pp. 033501, 2011, doi: 10.1063/1.3551583
6. Morozov, A. I., and Savelyev, V. V., "Fundamentals of Stationary Plasma Thruster Theory", *Review of Plasma Physics*, Vol. 21, pp. 203, 2000.
7. Mikellides, I.G., Katz, I, and Hofer, R.R, "Design of a laboratory Hall thruster with magnetically shielded channel walls, phase I: numerical simulations", AIAA paper 2011-5809, July 2011.
8. Hofer, R. R., Goebel, D. M., Mikellides, I. G., and Katz, I., "Design of a Laboratory Hall Thruster with Magnetically Shielded Channel Walls, Phase II: Experiments", AIAA paper 2012-3788, July 2012.
9. Haas, J. M., Hofer, R. R., Brown, D. L., B, Reid, B. M., and Gallimore, A. D., "Design of a 6-kW Hall thruster for high thrust/power investigation", in 54th JANNAF Propulsion Meeting, Denver, Colorado, 2007.
10. Lopez Ortega, A., Mikellides, I. G., and Chaplin, V. H., "Numerical Simulations for the Assessment of Erosion in the 12.5-kW Hall Effect Rocket with Magnetiuc Shielding (HERMeS)", IEPC-2017-154, October 2017.
11. Sekerak, J. M., Hofer, R. R., Polk, J. E., Jorns, B. A., and Mikellides, I. G., "Wear Testing of a Magnetically Shielded Hall Thruster at 2000-s Specific Impulse", IEPC 2015-155, July 2015.
12. Lopez Ortega, A., Mikellides, I. G., and Katz, I., "Hall2De Numerical Simulations for the Assessment of Pole Erosion in a Magnetically Shielded Hall Thruster", IEPC 2015-249, July 2015.

13. Jorns, B. A., Mikellides, I. G., and Goebel, D. M., "Ion Acoustic Turbulence in a 100-A LaB6 Hollow Cathode", Physical Review E, Vol. 90, 2014, 063106, doi: 10.1103/PhysRevE.90.063106
14. Jorns, B. A., Mikellides, I. G., Goebel, D. M., and Lopez Ortega, A., "Mitigation of Energetic Ions and Keeper Erosion in a High-current Hollow Cathode", IEPC-2015-134, in proceedings of the 34th International Electric Propulsion Conference, Hyogo-Kobe, Japan, July 2015
15. Polk, J. E., Lobbia, R. B., Barriault, A., Chaplin, V. H., Lopez Ortega, A., and Mikellides, I. G., "Inner Front Pole Erosion in the 12.5 kW HERMeS Hall Thruster over a Range of Operating Conditions", IEPC 2017-409, October 2017.
16. Jorns, B. A., Dodson, C. A., Anderson, R. A., Goebel, D. M., Hofer, R. R., Sekerak, J. M., Lopez Ortega, A. and Mikellides, I. G., " Mechanisms for Pole Piece Erosion in a 6-kW Magnetically Shielded Hall Thruster", AIAA paper 2016-4839, July 2016.
17. Chaplin, V. H, Jorns, B. A., Conversano, R. W., Lobbia, R. B., and Lopez Ortega, A., "Laser Induced Fluorescence Measurements of the Acceleration Zone in the 12.5 kW HERMeS Hall Thruster", IEPC 2017-229, October 2017.
18. Frieman, J. D., Ahern, D., Williams, G., Mackey, J., Haag, T., Huang, W., Kanhawi, H., Peterson, P. Y., Gilland, J. H., and Hofer, R. R., "In-situ Diagnostic for Assessing Hall Thruster Wear", AIAA paper 2018-xxxx, July 2018.
19. Huang, W., Kanhawi, H., and Herman, D. A., "Ion Velocity Distribution in the Channel and Near-Field of the HERMeS Hall Thruster", AIAA paper 2018-xxxx, July 2018
20. Mikellides, I. G. and Katz, I., "Numerical Simulations of Hall-effect Plasma Accelerators on a Magnetic-Field-Aligned Mesh", Physical Review E, Vol. 86, 2012, p. 046703, doi: 10.1103/PhysRevE.86.046703
21. Lopez Ortega, A. and Mikellides, I. G., "The Importance of the Cathode Plume and its Interactions with the Ion Beam in Numerical Simulations of Hall Thrusters", *Physics of Plasmas*, Vol. 23, 043515, 2016, doi: 10.1063/1.4947554
22. Katz, I. and Mikellides, I. G., "Neutral Gas Free Molecular Flow Algorithm Including Ionization and Walls for Use in Plasma Simulations", *Journal of Computational Physics*, Vol. 230, 2011, pp. 1454-1464, doi: 10.1016/j.jcp.2010.11.013
23. Stern, R. A., and Johnson, J. A. III. "Plasma Ion Diagnostics Using Resonant Fluorescence", *Physical Review Letters*, Vol. 34(25), pp. 1548-1551, 1975
24. Cedolin, R. J., Hargus, W. A., Storm, P. V., Hanson, R. K., and Cappelli, M. A., "Laser-Induce Fluorescence Study of a Xenon Hall Thruster", *Applied Physics B*, Vol. 65, pp. 459-469, 1997
25. Sullivan, R. M. Shepherd, J. E., Scharfe, M. K., Mikellides, I. G., and Johnson, L. K., "Effect of Wall Sheaths on Ion Trajectories in a Hall Thruster Numerical Model," IEPC-2009-131, July 2009.
26. Mikellides, I. G. and Lopez Ortega, A., "Assessment of Pole Erosion in a Magnetically Shielded Hall Thruster", AIAA-2014-3897, July 2014.
27. Hobbs, G. D., and Wesson, J. A., "Heat Flow through a Langmuir Sheath in Presence of Electron Emission," *Plasma Physics,* vol. 9, no. 1, pp. 85-87, 1967.
28. Lopez Ortega, A. and Mikellides, I. G., "Hall2De numerical simulations for the assessment of pole erosion in a magnetically shielded Hall thruster", in preparation, 2018
29. Lopez Ortega, A., Mikellides, I. G., and Goebel, D. M., "OrCa2D Simulations for Life Assessments of the BaO and LaB6 Hollow Cathode Options in the Hall Effect Rocket with Magnetic Shielding", IEPC paper 2017-152, October 2017.